

fMRI-LM: Towards a Universal Foundation Model for Language-Aligned fMRI Understanding

Yuxiang Wei
TreNDS
weiyuxiang@gatech.edu

Yanteng Zhang
TreNDS

Xi Xiao
University of Alabama at Birmingham

Chengxuan Qian
Jiangsu University

Tianyang Wang
University of Alabama at Birmingham

Vince D. Cahoun
TreNDS
vcalahoun@gatech.edu

Abstract

Recent advances in multimodal large language models (LLMs) have enabled unified reasoning across images, audio, and video, but extending such capability to brain imaging remains largely unexplored. Bridging this gap is essential to link neural activity with semantic cognition and to develop cross-modal brain representations. To this end, we present **fMRI-LM**, a foundational model that bridges functional MRI (fMRI) and language through a three-stage framework. In Stage 1, we learn a neural tokenizer that maps fMRI into discrete tokens embedded in a language-consistent space. In Stage 2, a pretrained LLM is adapted to jointly model fMRI tokens and text, treating brain activity as a sequence that can be temporally predicted and linguistically described. To overcome the lack of natural fMRI-text pairs, we construct a large descriptive corpus that translates diverse imaging-based features into structured textual descriptors, capturing the **low-level organization** of fMRI signals. In Stage 3, we perform multi-task, multi-paradigm instruction tuning to endow fMRI-LM with **high-level semantic** understanding, supporting diverse downstream applications. Across various benchmarks, fMRI-LM achieves strong zero-shot and few-shot performance, and adapts efficiently with parameter-efficient tuning (LoRA), establishing a scalable pathway toward a language-aligned, universal model for structural and semantic understanding of fMRI.

1. Introduction

Functional magnetic resonance imaging (fMRI) provides a noninvasive window into human brain activity by capturing blood-oxygen-level-dependent (BOLD) fluctuations across

* Preliminary work. Codes and model checkpoints will be publicly available soon.

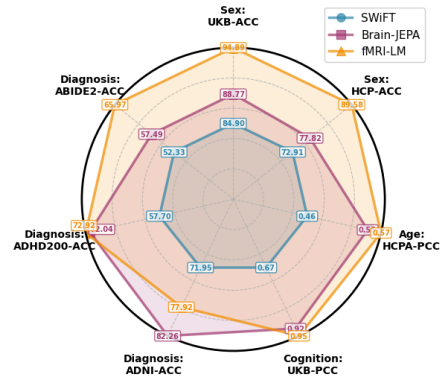


Figure 1. The proposed fMRI-LM outperforms baselines on diverse tasks. fMRI-LM demonstrates comprehensive and powerful performance.

distributed regions. Deep learning has achieved strong performance on supervised fMRI tasks such as phenotype prediction and disease diagnosis [3, 17, 19, 20, 23, 35], but these models typically require task-specific tuning and labeled data, limiting scalability and cross-study generalization. Recent fMRI foundation models, such as BrainLM and Brain-JEPA [5, 9], pretrain on large neuroimaging corpora and transfer well to downstream tasks, yet they remain confined to neural-only objectives (e.g., masked prediction, contrastive learning), requires task-specific tuning, and lack grounding in language.

In parallel, large language models (LLMs) and multi-modal LLMs (MLLMs) have demonstrated strong cross-modal reasoning over images, audio, and video [4, 21, 22, 37]. MLLMs typically pair an off-the-shelf LLM with a modality-specific encoder whose outputs are aligned with the text embedding space. Inspired by this design, recent work on EEG [14, 15] treats neural signals as a kind of “language” by quantizing activity into symbolic representations

and aligning them with pretrained LLMs. However, these approaches mainly rely on fixed single-question–single-answer templates, underutilizing LLMs’ generative and reasoning capabilities; they also focus on EEG rather than fMRI, and the absence of natural fMRI–text pairs prevents modeling of linguistic semantics that describe brain function. Although several recent works employ LLMs for fMRI-to-text decoding [28, 36], they are tailored to task-fMRI settings with explicit stimulus–text pairs and primarily use the LLM’s embedding space to map neural activity back to presented text. In contrast, our goal is to develop a generalizable fMRI foundation model that understands *resting-state and task-independent* neural patterns, without relying on task-evoked paired text.

To explore the potential of LLMs for universal fMRI understanding, we propose **fMRI-LM**, a foundational model that bridges fMRI and language through a unified multi-stage framework. fMRI-LM is pretrained on over 50,000 fMRI scans spanning a wide age range. A key component is a **structured fMRI–text corpus** that converts imaging-derived features—functional connectivity, graph-theoretical metrics, functional gradients, and ICA (independent component analysis) components—into standardized textual descriptions, providing language-grounded access to the *low-level structure* of fMRI, understood as pre-semantic patterns of connectivity and functional organization analogous to low-level spatial and textural features in images. In Stage 1 (**fMRI tokenizer training**), a Transformer-based tokenizer with vector quantization maps fMRI into token embeddings aligned with the LLM’s text embedding space. In Stage 2 (**LLM fine-tuning**), a pretrained LLM is tuned to model fMRI tokens and synthetic fMRI–text pairs, enabling both temporal modeling of brain activity and fMRI-conditioned text generation. Stage 3 (**downstream instruction tuning**) performs multi-task, multi-paradigm instruction tuning—covering single- and multi-question answering and open-ended description generation—to endow fMRI-LM with *high-level semantic understanding* across diverse neuroscience and clinical tasks. As summarized in Fig. 1, fMRI-LM outperforms strong baselines on a range of benchmarks.

Our key insight is that this descriptive corpus forms a bridge between low-level neural organization and high-level cognitive semantics, analogous to how captions connect image structure to scene meaning in vision–language models. By aligning fMRI with language through this corpus, fMRI-LM learns representations that are transferable across datasets, subjects, and tasks. Overall, our contributions are:

- We introduce **fMRI-LM**, to our knowledge the first LLM-aligned foundational framework for fMRI that maps resting-state and task-independent brain activity into a token space compatible with pretrained language models, enabling a unified interface for fMRI modeling

and instruction tuning.

- We construct a large-scale **descriptive corpus** that translates fMRI imaging-based features into structured, caption-like text, providing language supervision that helps the LLM capture the low-level organization and interpretable structure of fMRI signals.
- We show that fMRI-LM **significantly outperforms** supervised and foundation baselines on standard benchmarks, while exhibiting strong **generalization** across tasks and datasets. Moreover, the model shows notable **efficiency**, delivering strong results even with limited training data and a small fraction of tunable parameters.

2. Related Work

Brain-LLM Alignment and Convergent Representations: Recent large-scale analyses reveal that high-performing deep learning models, particularly LLMs, naturally develop representations that align with brain activity. Shen [31] found that brain–model alignment strongly correlates with task performance and even precedes capability gains during training. Likewise, Badr [2] suggested that LLMs develop brain-like representations for language and eventually outgrow linguistic rules. Such convergent evolution between biological and language model intelligence indicates that language models may capture representational structures more consistent with human cognition. Motivated by this, we hypothesize that LLMs provide a strong semantic prior for modeling fMRI signals and can enable richer interpretations than task-specific architectures.

Foundation Models for fMRI Understanding: Recent work in fMRI analysis has shifted from task-specific prediction to general representation learning, driving the development of foundation models that extract transferable neural features from large-scale data. The early supervised CNN and GNN-based approaches performed well in diagnostic tasks but generalized poorly across cohorts [16, 17, 19, 20, 23]. Recent self-supervised models such as BrainLM [5] and Brain-JEPA [9] improve robustness by pretraining with masked reconstruction or contrastive objectives before task-specific fine-tuning. However, these models remain task-bound and lack semantic grounding. Our work addresses this gap by aligning fMRI representations with an LLM backbone to enable unified, language-informed understanding of brain activity.

3. Methodology

In this section, we explain the modules and training pipeline of fMRI-LM. As illustrated in Fig. 4, we first train an fMRI tokenizer composed of a ViT-based encoder [9] and a quantizer [25, 34] that produces fMRI tokens aligned with the frozen text space. A pretrained LLM is then tuned to predict the fMRI tokens and text tokens, followed by supervised in-

Table 1. fMRI-text descriptors

type	level	name
FC	ROI	Network-pair connectivity
	Global	Top/bottom connectivity patterns
FG	ROI	Network gradient values
	Global	Principal/second/third gradient range
	Global	Gradient variance
ICA	ROI	Network temporal amplitude, variability, spectral ratio
	ROI	Network-pair FNC
	ROI	Network fALFF
	Global	Overall temporal amplitude, variability, spectral ratio
Graph	ROI	Network strength
	Global	Modularity, global efficiency, average clustering coefficient

struction tuning.

Given the 4D fMRI $X_{\text{raw}} \in \mathbb{R}^{T \times X \times Y \times Z}$, we follow previous works [5, 9] and parcellate into ROI-level fMRI signals based on atlas Schaefer-400 [30] for cortical regions and Tian-Scale III [33] for subcortical regions, resulting in $N = 450$ ROIs: $X \in \mathbb{R}^{T \times N}$.

3.1. fMRI-Text Descriptor Construction

In common vision–language model training, each image is paired with one or more textual descriptions that capture its spatial structure and semantic content. Such captions provide a bridge between visual and linguistic representations, enabling effective multimodal alignment. However, due to the abstract and high-dimensional nature of fMRI data, no analogous text descriptions exist in prior studies.

To address this challenge, we curate a structured text corpus that describes each fMRI data in terms of four complementary feature domains: *functional connectivity (FC)*, *functional gradient (FG)*, *graph-theoretical metrics*, and *independent component analysis (ICA)*. Each description summarizes both the region-of-interest (ROI)–level and global characteristics derived from these representations, as detailed in Tab. 1. All functional brain measures are z-scored and normalized relative to the cohort distribution (UK Biobank) to enable interpretable, standardized comparisons across subjects. The quantitative values are then fit to a template to generate cohesive text descriptions. Together, these descriptors capture diverse aspects of intrinsic brain organization and serve as linguistic analogs of neural representations, facilitating multimodal alignment with language models. Complete explanations and the meaning of each descriptor are elucidated in **Appendix A**. To ensure the descriptors contain meaningful information, we train a BERT classifier [7] with the 4 types of descriptors for UKB sex prediction and compare it with the BrainNetCNN [19] model, as presented in Fig. 3.

Subject attributes such as demographics are widely used to enhance downstream task accuracy, especially disease diagnosis [35, 38]. We further utilize the demographics, phenotypical, cognitive, and physical attributes to construct high-level subject descriptions. These semantic descriptions are only used in Stage 3 disease- and cognition-related

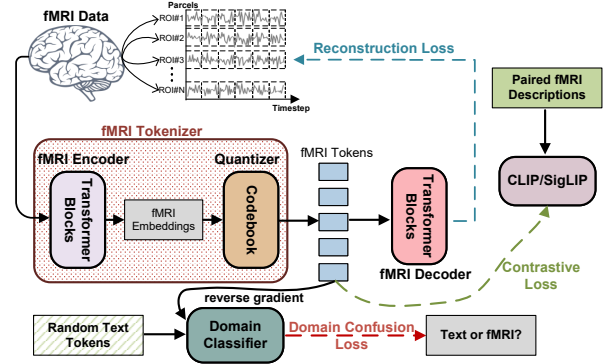


Figure 2. Overview of the fMRI tokenizer, which consists of a Transformer-based encoder and a vector quantizer. The tokenizer is trained with reconstruction, domain-adversarial, and contrastive alignment losses to align fMRI representations with the LLM’s text-embedding space.

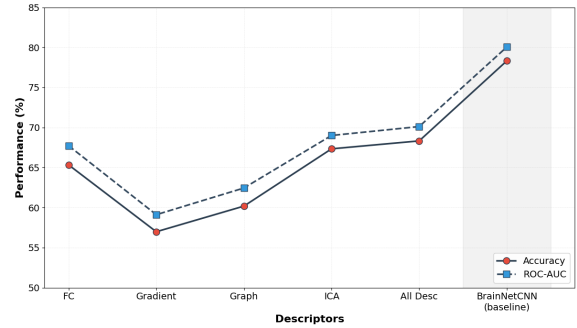


Figure 3. Descriptors’ predictive strength over UKB sex. Using all descriptors (“All Desc”) can achieve about 70% accuracy.

tasks only. Further details are given in Sec. 4.1 and in **Appendix A.5**.

3.2. Text-Aligned fMRI Tokenizer

To enable pretrained LLMs to understand non-text modalities, it is essential to first encode the input data into embeddings that are *aligned with the frozen text space*. We therefore design a text-aligned fMRI tokenizer, which maps fMRI signals into discrete neural tokens that share a consistent representational geometry with language embeddings.

Architecture. We employ a Transformer-based encoder \mathcal{E}_θ inspired by recent neural encoding frameworks [9], followed by a vector quantizer to discretize the continuous embeddings. As shown in Fig. 2, given an fMRI input $X \in \mathbb{R}^{T \times N}$, the encoder $\mathcal{E}_\theta(\cdot)$ produces a latent feature sequence $z = \mathcal{E}_\theta(X)$, where $z \in \mathbb{R}^{M \times C}$, C denotes the embedding dimension, and $M = \lceil \frac{T}{P} \rceil \times N = T' \times N$ is the sequence length. The patch size P is applied only along the temporal dimension to preserve all ROI features.

A quantization module \mathcal{Q} , then maps each continuous latent vector z_m to a discrete representation \tilde{z}_m . This module can be implemented using various schemes, such as stan-

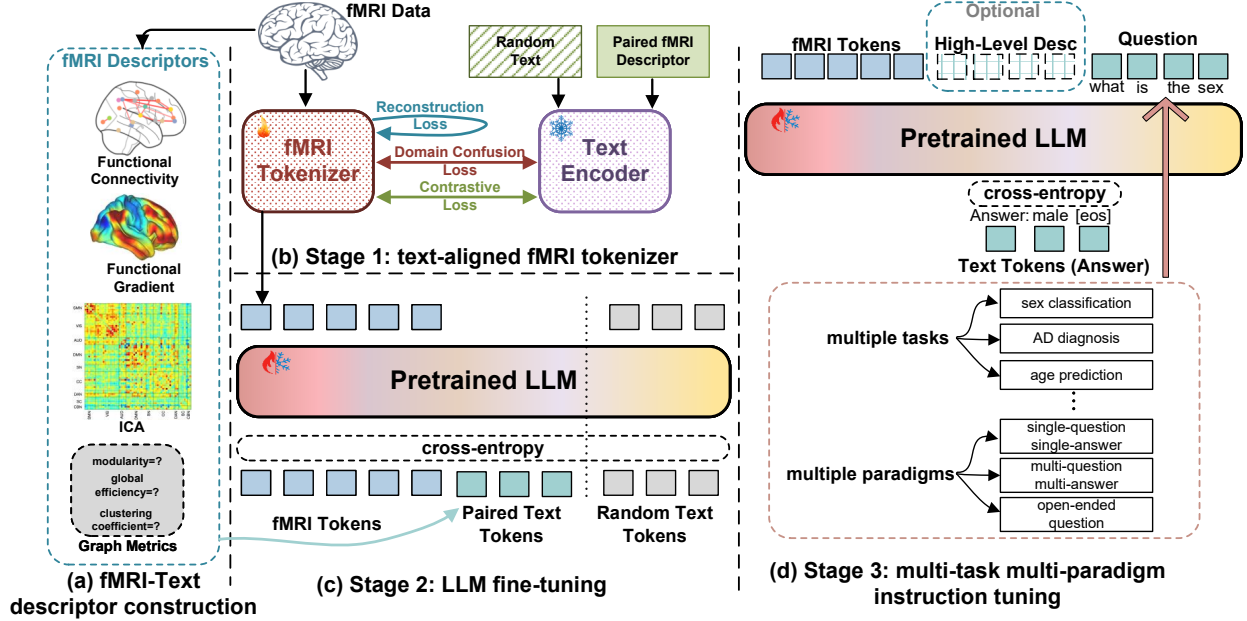


Figure 4. Overall training pipeline of **fMRI-LLM**. (a) fMRI–text pairs are constructed from four types of features: functional connectivity, graph metrics, functional gradients, and ICA-based components. (b) *Stage 1*: align the fMRI tokenizer with the frozen text embedding space. (c) *Stage 2*: tune a pretrained LLM to generate linguistic or temporal representations conditioned on fMRI tokens. Use either full fine-tuning or LoRA [13]. (d) *Stage 3*: multi-task multi-paradigm instruction tuning for downstream tasks. High-level descriptions are used as optional input for enhanced performance.

dard vector quantization (VQ) [34]. The resulting sequence $\tilde{z} = [\tilde{z}_1, \dots, \tilde{z}_M]$ serves as discrete fMRI representation.

To preserve information fidelity, a lightweight decoder \mathcal{D}_ϕ is trained to reconstruct the original input. The objective for the tokenizer’s autoencoding component is:

$$\mathcal{L}_{\text{quant}} = \|X - \mathcal{D}_\phi(\tilde{z})\|_2^2 + \mathcal{L}_{\text{commitment}}, \quad (1)$$

where the first term is the reconstruction loss and $\mathcal{L}_{\text{commitment}}$ is a regularizing term depends on \mathcal{Q} .

Domain-Adversarial Alignment. Following the domain adaptation strategy of [11, 14], we align fMRI embeddings with the text-embedding space of a pretrained LLM. Specifically, we sample text embeddings $z_{\text{text}} \in \mathbb{R}^{M \times C}$ from a frozen LLM (e.g., GPT-2) using tokens drawn from OpenWebText [12]. A domain classifier \mathcal{C} is trained to discriminate whether a given embedding originates from fMRI or text, while a gradient reversal layer (GRL) is applied between \mathcal{E}_θ and \mathcal{C} to enforce confusion. The domain-adversarial loss is defined as

$$\mathcal{L}_{\text{domain}} = -\frac{1}{M} \sum_{m=1}^M \left[t_m \log \mathcal{C}(z_m) + (1-t_m) \log(1-\mathcal{C}(z_m)) \right] \quad (2)$$

where $t_m = 1$ if the sample is from fMRI and $t_m = 0$ otherwise. This adversarial objective encourages the fMRI tokenizer to produce embeddings that are indistinguishable from text embeddings in the LLM space.

Contrastive Cross-Modal Alignment. To further bridge the modality gap, we leverage the synthetic text descriptors introduced in Sec. 3.1 to form paired fMRI–text data. We employ a SigLIP-style contrastive loss [40], which maximizes similarity between paired embeddings while minimizing it across unpaired samples:

$$\mathcal{L}_{\text{contrast}} = -\frac{1}{B} \sum_{i=1}^B \log \frac{\exp(\sigma \cdot \text{sim}(z_i, z_i^+))}{\sum_{j=1}^B \exp(\sigma \cdot \text{sim}(z_i, z_j^+))} \quad (3)$$

where $\text{sim}(\cdot, \cdot)$ denotes cosine similarity, z_i and z_i^+ represent matched fMRI and text features, σ is a temperature parameter, and B is the batch size.

Overall Objective. The final loss for the text-aligned fMRI tokenizer combines reconstruction, domain-adversarial, and contrastive terms:

$$\mathcal{L}_{\text{tokenizer}} = \mathcal{L}_{\text{quant}} + \mathcal{L}_{\text{contrast}} + \lambda \mathcal{L}_{\text{domain}} \quad (4)$$

where λ is empirically set to 0.5. Through this joint optimization, the tokenizer learns discrete neural tokens that both preserve fMRI structure and align closely with the semantic geometry of text embeddings.

3.3. LLM Fine-Tuning and Temporal Modeling

Given discrete fMRI tokens, we fine-tune a pretrained LLM to model temporal dynamics and generate text. Let $\mathbf{z} =$

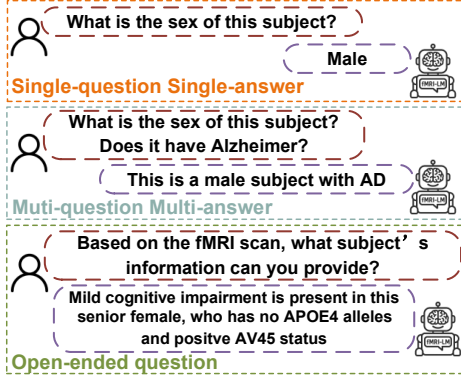


Figure 5. Three paradigms for instruction tuning

$\{z^{(w,n)}\}$ denote the token sequence, where $w = 1, \dots, T'$ is the time index and $n = 1, \dots, N$ indexes ROIs, and let $I^{(w,n)} \in \mathcal{V}$ be the corresponding vocabulary indices generated from the quantizer.

Model Input and Objectives. Unlike standard language modeling, where the model predicts the next word in a textual sequence, fMRI data exhibit a *temporal-spatial* structure. Inspired by [14], we adapt the LLM to perform **temporal next-step prediction**. Formally, given tokens from N ROIs at time w , the LLM predicts the N tokens at $w + 1$.

To endow the LLM with both neural and linguistic competence, we introduce three complementary training paradigms as illustrated in Fig. 4(c):

- fMRI-to-fMRI (F2F): temporal next-step prediction of fMRI tokens using Eq. (5):

$$\mathcal{L}_{\text{F2F}} = - \sum_{w=1}^{T'-1} \sum_{n=1}^N \log P_{\theta} \left(I^{(w+1,n)} \mid \mathbf{z}^{(w,1)}, \dots, \mathbf{z}^{(w,N)} \right) \quad (5)$$

where θ denotes the LLM parameters and P_{θ} represents the autoregressive probability distribution over the extended vocabulary. This objective encourages the LLM to capture temporal dependencies in neural activity.

- fMRI-to-Text (F2T): conditioned text generation, where the model learns to produce descriptive text tokens given an fMRI token sequence.
- Text-to-Text (T2T): standard language modeling with random text to preserve LLM’s original linguistic ability.

The combined loss for LLM alignment is thus:

$$\mathcal{L}_{\text{LLM}} = \mathcal{L}_{\text{F2T}} + \alpha \mathcal{L}_{\text{F2F}} + \beta \mathcal{L}_{\text{T2T}} \quad (6)$$

where α and β are empirically set to 0.1 and 0.5.

3.4. Multi-Task Multi-Paradigm Instruction Tuning

Foundational vision-language models benefit greatly from diverse instruction-tuning objectives, which enable strong

generalization across heterogeneous tasks [32]. To enable flexible reasoning across diverse neuroscience and clinical tasks, we perform **multi-task, multi-paradigm instruction tuning** on top of the aligned LLM (Stage 3). Tasks are presented as natural-language queries paired with target responses, covering phenotype prediction, cognitive state classification, and disease diagnosis.

We adopt three paradigms (Fig. 5): (i) single-question single-answer, (ii) multi-question multi-answer, and (iii) open-ended description. The open-ended setting instructs the model to produce free-form text (e.g., interpreting subject characteristics), encouraging generalizable semantic understanding. Detailed prompt formats and task definitions are provided in **Appendix D**.

Importantly, the three paradigms are designed primarily as complementary *evaluation* protocols with increasing difficulty, not as a way to enlarge the instruction-tuning corpus. They reuse the same underlying supervision (labels and attributes) but present it under different interaction formats, allowing us to probe how well fMRI-LM handles basic prediction, multi-target reasoning, and free-form generation.

4. Experiments

4.1. Experimental Settings

Datasets. We primarily focus on resting-state fMRI due to its wide availability and standardized acquisition protocols. Two large-scale public datasets—UK Biobank (UKB) [26] and Adolescent Brain Cognitive Development (ABCD) [18]—are used in stage 1 and 2. Each dataset is randomly split with an 80%–20% ratio for pretraining and held-out downstream evaluation. To assess generalization and zero-shot transfer, we further include six external datasets spanning multiple age groups and clinical conditions, as summarized in Tab. 2.

Since these datasets vary in spatial and temporal resolutions across imaging sites, we standardize all data to ensure consistent temporal resolution and input shape. Specifically, we resample all fMRI time series to a repetition time (TR) of 2.0 s and clip or linearly interpolate each sequence to 160 time points, with 450 ROIs extracted using Schaefer-400 and Tian-Scale III atlases [30, 33]. Before feeding the data into the tokenizer, we perform robust z-score normalization across time for each ROI and apply site-wise variance normalization to mitigate scanner-related biases.

Paired fMRI-Text Curation and Prompt Expansion. To construct paired fMRI-text data, we generate imaging-based textual descriptors for each scan in UKB. Each scan is represented by 23 descriptors derived from four domains, as described in Sec. 3.1. We use fixed templates to convert numerical statistics into natural-language statements, which are subsequently refined into cohesive paragraphs using DeepSeek-V3 [24]. Subject-level semantic descriptions

Table 2. Dataset summary. Datasets marked with * are also used for zero-/few- shot evaluation. More details in **Appendix B**.

Dataset	Size	Age Group	Task
UKB* [26]	39305	37-87	Sex, Age, Fluid Intel
ABCD [18]	18337	9-11	Sex
HCP [10]	1079	22-37	Sex, Age, Fluid Comp
HCP-A* [10]	632	36-100	Sex, Age, Fluid Comp, Flanker
ADNI4 [27]	1030	55-90	Sex, Age, AD, Apoe4
ADHD200* [6]	624	7-22	ADHD
ABIDE2* [8]	1114	5-64	Autism

are similarly synthesized from demographic and diagnostic attributes to capture broader cognitive or clinical information. More information is in **Appendix A**.

For instruction tuning, we develop a diverse set of prompts to improve generalization and linguistic robustness. Each downstream paradigm is augmented with up to 200 paraphrased prompt variants generated via LLM rewriting. In training, a random subset of prompts is sampled at each iteration to avoid overfitting to specific phrasings.

Implementation Details. We introduce three model sizes, **fMRI-LM-S**, **fMRI-LM-B**, and **fMRI-LM-L** with trainable parameters of 46M, 174M, and 610M, respectively (excluding the base LLM). The tokenizer employs a Transformer encoder with a temporal patch size of 32 and a vanilla vector quantizer [34], although other quantizers (e.g., FSQ [25]) can be substituted. Unless otherwise stated, we report results for fMRI-LM-B with GPT-2 (124M) [29].

All three stages are trained for 50 epochs using AdamW with a learning rate of 10^{-4} , cosine-annealing scheduler, and batch size of 32. In Stage 1, we freeze the text encoder and train only the fMRI tokenizer. In Stages 2 and 3, the tokenizer is frozen while the LLM is tuned using either full fine-tuning or parameter-efficient LoRA [13]. More details on training hyperparameters can be found in **Appendix C**.

4.2. Main Results

In this section, we systematically evaluate fMRI-LM to answer the following questions: **Baseline Comparison:** Can fMRI-LM surpass SOTA baselines on standard single-question tasks? **Versatility:** Does instruction tuning allow for diverse formats without performance loss? **Generalization:** Does the model demonstrate zero- **Efficiency:** Is the model effective under data and tuning parameter constraints?

Single-Question Single-Answer. We first evaluate fMRI-LM-B with GPT-2 and Qwen3-0.6B backbones under the single-question single-answer paradigm, and compare against supervised and foundation models for fMRI. Note that fMRI-LM is tuned jointly on the 5 datasets. For regression targets, the tokenized output space of LLMs is inherently discrete and thus poorly suited for directly predicting continuous values. We therefore adopt two strategies: (i) linear probing [1] with a lightweight prediction head on top

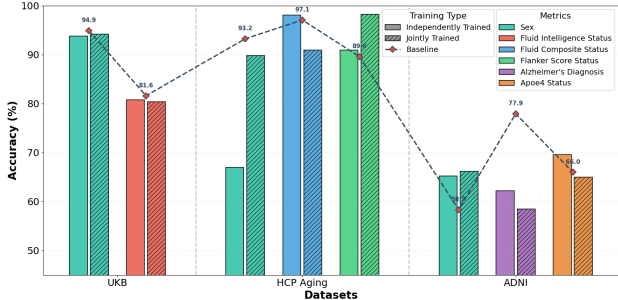


Figure 6. Performance of fMRI-LM on the multi-question multi-answer across UKB, HCP-A, and ADNI. We report results when training independently on each dataset and when jointly training on all three. "baseline" refers to single-question single-answer.

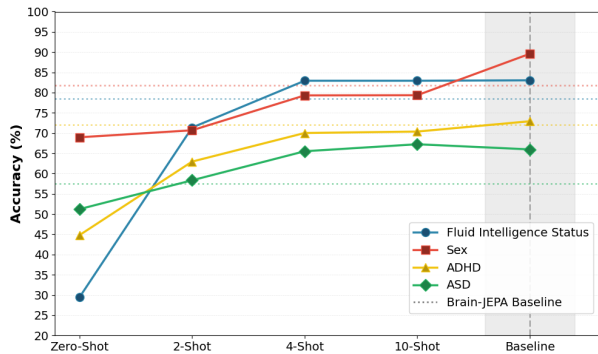


Figure 7. Zero-shot and few-shot generalization of fMRI-LM. We evaluate three settings: new task on the same dataset, same task on a new dataset, and new task on a new dataset. "baseline" refers to single-question single-answer.

of the LLM’s hidden representations, and (ii) discretizing continuous variables into ordinal bins and formulating them as classification, allowing the model to output faithful discrete responses. Details of the discretization and additional results are provided in **Appendices B, E, and F**.

As shown in Tab. 3 and Tab. 4, the two variants of fMRI-LM achieve the best or second-best performance on most datasets and targets. Although fMRI-LM underperforms Brain-JEPA on ADNI-AD, we emphasize that the key strength of our framework is its unified instruction-tuning pipeline and its ability to handle diverse tasks without extensive task-specific fine-tuning.

Multi-Question Multi-Answer. We next evaluate the multi-question multi-answer paradigm, where each fMRI scan is paired with multiple questions and the model must predict all answers simultaneously. We report results on UKB, HCP-A, and ADNI, as summarized in Fig. 6. Detailed definitions of each target and its possible values are provided in **Appendix D.2**.

Compared to the single-question setting, perfor-

Table 3. Compare fMRI-LM with supervised methods and foundation models on classification tasks. Bold denotes the best method and underline denotes the 2nd best. Note: fMRI-LM-B(G) denotes fMRI-LM-B(GPT2).

Type	Method	UKB-Sex		HCP-Sex		ADNI-AD		ADHD200-ADHD		ABIDE2-ASD	
		Acc	AUC								
Supervised	BrainNetCNN [19]	78.32 (1.12)	80.05 (1.06)	82.01 (2.11)	86.94 (1.64)	75.92 (2.24)	77.09 (1.62)	52.19 (3.14)	56.21 (2.82)	56.32 (2.45)	57.82 (2.51)
	BrainGNN [23]	77.31 (2.47)	79.53 (1.46)	79.09 (1.81)	81.56 (0.49)	68.72 (2.84)	69.06 (3.11)	55.67 (2.49)	56.72 (1.69)	57.02 (2.67)	58.09 (3.73)
	BNT [17]	72.71 (2.64)	73.38 (1.92)	72.67 (1.49)	72.05 (1.32)	70.19 (3.20)	72.34 (2.25)	55.54 (2.39)	57.05 (3.32)	52.19 (3.10)	54.22 (2.44)
	FBNETGEN [16]	83.54 (4.67)	83.56(2.67)	80.64 (2.41)	79.29 (3.91)	76.74 (2.55)	77.64 (1.09)	49.18 (1.76)	52.42 (2.69)	51.12 (1.36)	54.65 (2.08)
	SWIFT [20]	84.90 (1.88)	85.34 (3.19)	72.91 (1.49)	71.69 (1.64)	71.95 (2.22)	70.08 (1.5UY9)	57.70 (2.44)	58.04 (1.88)	52.33 (2.21)	55.46 (2.72)
Foundation	BrainLM [5]	88.72 (0.88)	90.42 (0.59)	81.09 (1.76)	82.34 (2.21)	78.82 (1.54)	75.21 (1.68)	71.22 (1.49)	65.21 (1.68)	<u>65.22</u> (2.28)	<u>67.29</u> (1.18)
	BrainMass [39]	92.31 (0.19)	92.85 (0.22)	75.32 (0.49)	77.19 (1.01)	80.05 (2.21)	83.35 (1.98)	66.19 (2.27)	62.24 (1.79)	58.79 (1.12)	63.48 (1.79)
	Brain-JEPA [9]	88.77 (0.75)	90.13 (0.63)	77.82 (1.12)	79.19 (1.62)	82.26 (2.17)	84.05 (2.64)	72.04 (2.39)	65.18 (2.42)	57.49 (1.49)	64.28 (1.95)
	fMRI-LM-B(G)	94.89 (0.22)	94.90 (0.16)	<u>89.58</u> (0.31)	<u>89.13</u> (0.79)	77.92 (1.01)	79.91 (1.25)	<u>72.92</u> (1.34)	<u>68.72</u> (2.01)	65.97 (1.09)	68.72 (1.33)

Table 4. Compare fMRI-LM with supervised methods and foundation models on regression tasks. Bold denotes the best method and underline denotes the 2nd best. Note: fMRI-LM-B(G) denotes fMRI-LM-B(GPT2).

Method	UKB				HCP				HCP-Aging			
	Age		Fluid Intel		Age		Fluid Comp		Flanker		Fluid Comp	
	MAE↓	p↑	MAE↓	p↑	MAE↓	p↑	MAE↓	p↑	MAE↓	p↑	MAE↓	p↑
SwiFT	3.40 (0.21)	0.49 (0.073)	1.85 (0.092)	0.67 (0.011)	2.58 (0.25)	0.51 (0.046)	5.15 (0.39)	0.62 (0.11)	6.85 (0.44)	0.19 (0.035)	5.32 (0.26)	0.59 (0.067)
BrainMass	2.01 (0.052)	0.77 (0.063)	1.59 (0.039)	0.88 (0.016)	3.01 (0.19)	0.49 (0.052)	5.29 (0.84)	0.55 (0.20)	5.66 (0.75)	0.40 (0.016)	5.05 (0.49)	0.58 (0.16)
Brain-JEPA	1.69 (0.088)	<u>0.76</u> (0.10)	1.59 (0.042)	<u>0.92</u> (0.011)	2.55 (0.15)	0.62 (0.069)	4.87 (0.096)	0.70 (0.062)	5.21 (0.13)	0.44 (0.036)	4.88 (0.056)	<u>0.73</u> (0.074)
fMRI-LM-B(G)	1.82 (0.061)	0.85 (0.034)	<u>1.51</u> (0.011)	0.95 (0.006)	<u>2.56</u> (0.13)	0.62 (0.11)	<u>4.68</u> (0.25)	<u>0.74</u> (0.033)	5.11 (0.075)	0.50 (0.006)	<u>4.70</u> (0.29)	0.76 (0.029)

mance under the multi-question paradigm degrades only marginally relative to strong baselines, with the largest drop observed for AD prediction on ADNI. In contrast, fMRI-LM achieves comparable or even higher accuracy on several targets (e.g., sex, fluid composite, and flanker scores), suggesting that jointly training on multiple, potentially correlated targets can help the model acquire more universal fMRI representations and solve a broader set of tasks.

Open-Ended Question. We further evaluate fMRI-LM on open-ended questions on UKB, HCP-A, and ADNI, as shown in Fig. 8. All datasets share three common target fields, and each dataset additionally includes a small set of unique targets. The “overall” metric requires all fields in a generated sentence to match the ground-truth labels in order for the prediction to be counted as correct. Detailed definitions are given in **Appendix D.3**.

Since the model is tuned to generate cohesive free-form text instead of structured single or multiple answers, we employ DeepSeek-V3 as an automatic evaluator to determine whether the generated answer matches the target fields, and subsequently perform manual verification by human experts. From Fig. 8, fMRI-LM performs surprisingly well on several targets such as sex and fluid composite status, achieving accuracy comparable to the structured paradigms. Jointly training across datasets (except for ADNI, likely due to its biomarker-driven, disease-specific distribution differing from the others) further improves performance, indicating that fMRI-LM benefits from task and dataset diversity and can develop more universal fMRI understanding.

Zero-Shot and Few-Shot Generalization. We finally test whether fMRI-LM can generalize to unseen tasks or datasets with no or limited labeled data (2, 4, and 10 samples, balanced by label). We explore three configurations: (i) new task on the same dataset, (ii) same task on a new dataset, and (iii) new task on a new dataset. Concretely, we first train the model on UKB for sex classification, then evaluate its zero-shot and few-shot performance on fluid intelligence status prediction in UKB, sex classification on HCP-A, disease-related tasks on ADHD200 and ABIDE2.

As shown in Fig. 7, fMRI-LM performs relatively poorly in the strict zero-shot setting, but its performance improves substantially even with only two labeled samples. This suggests that the model learns general fMRI representations can be quickly adapted with minimal supervision. Notably, fMRI-LM attains performance comparable to using the full downstream training set under a 4-shot setting for fluid intelligence status prediction and ASD prediction, indicating that the model does not rely heavily on large downstream datasets and can flexibly adapt to a wide variety of tasks.

4.3. Ablation Studies

More ablations on model size and loss configurations are provided in **Appendix G**.

Effect of Imaging-Based and Semantic Descriptors. To assess the contribution of the imaging-based descriptors introduced in Sec. 3.1 and **Appendix A**, we evaluate fMRI-LM without any paired fMRI-text data during pretraining (i.e., removing the contrastive loss in Eq. (3) and the F2T

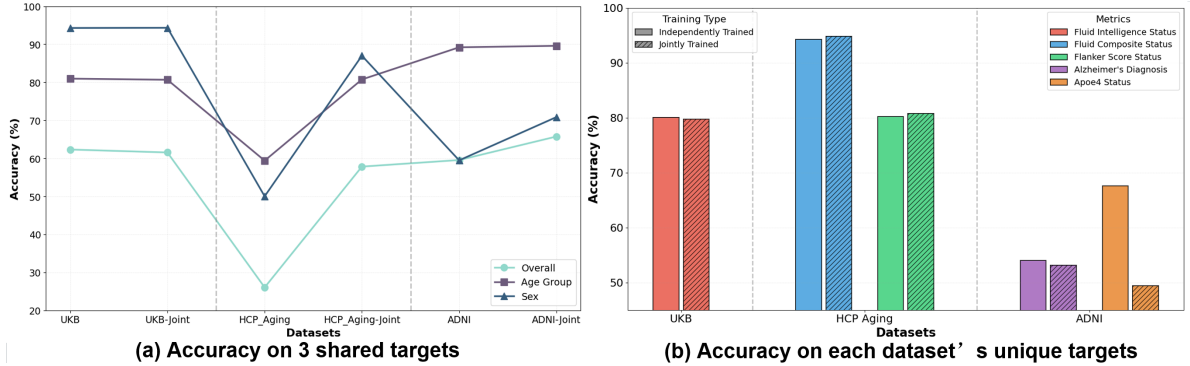


Figure 8. Open-ended question performance of fMRI-LM on UKB, HCP-A, and ADNI. We show models trained independently on each dataset as well as a jointly trained model. “Baseline” indicates performance on each target under the single-question single-answer setting.

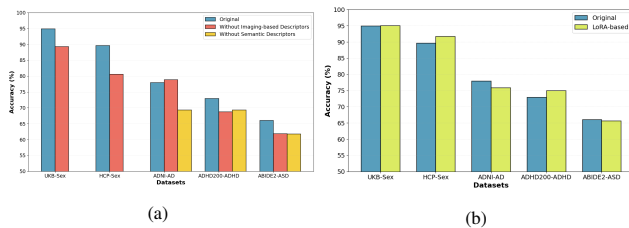


Figure 9. (a) Effect of imaging-based and semantic descriptors. Semantic descriptors are only used for disease- and cognition-related tasks. (b) Effect of LoRA-based tuning on fMRI-LM.

objective in Sec. 3.3). We also ablate the high-level semantic text descriptions used as complementary input during downstream tuning. The results are shown in Fig. 9(a). Removing the imaging-based descriptors—and thus the fMRI–text pairs used during pretraining—significantly degrades performance, especially on sex classification. While performance on ADNI-AD slightly improves after removal, we hypothesize this is due to distributional differences between the pretraining data (UKB/ABCD) and ADNI’s disease-focused population, which may reduce the benefit of descriptor-based alignment in this specific case.

Parameter-Efficient Tuning via LoRA. While full fine-tuning of LLMs is effective, it can be computationally demanding and prone to overfitting with limited data. To address this, we investigate a parameter-efficient fine-tuning approach using Low-Rank Adaptation (LoRA) [13] for Stages 2 and 3. As shown in Fig. 9(b), employing LoRA not only maintained but in some cases, improved performance on tasks such as HCP sex classification and ADHD diagnosis. This suggests that LoRA effectively adapts the model to fMRI data by tuning only a small fraction of its parameters. This approach preserves the rich linguistic knowledge encoded in the pretrained LLM, which is crucial for strong performance, while efficiently learning the relevant neuro-semantic representations from the fMRI inputs.

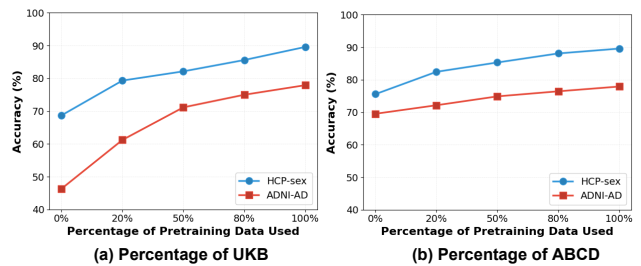


Figure 10. Effect of pretraining data size on downstream performance for HCP sex classification and ADNI AD prediction.

Impact of Pretraining Data Size. To explore the effect of pretraining data scale, we vary the fraction of UKB and ABCD used for pretraining (from 0% to 100%) and evaluate downstream performance on HCP sex classification and ADNI AD prediction. As shown in Fig. 10, even without UKB or ABCD, the model achieves reasonable performance (around 70% for sex and 50% for AD). Removing ABCD has smaller impact than removing UKB, which may be attributed to domain shift (ABCD focuses on children, while most other datasets focus on adults). Overall, performance improves consistently with more pretraining data.

5. Conclusion

We introduced fMRI-LM, a foundational framework for universal fMRI understanding that aligns fMRI with LLMs through the synthetic fMRI–text descriptor corpus, which provides scalable linguistic supervision in the absence of natural fMRI–text pairs. Extensive experiments across seven datasets demonstrate fMRI-LM’s strong performance and generalization, with further ablation studies validating the importance of paired descriptors and confirming its adaptability and scalability, even under parameter-efficient (LoRA) and few-shot settings. This work presents a step toward unified, language-grounded brain modeling. By leveraging

the structure and reasoning capabilities of LLMs, it offers a scalable way to interpret fMRI, integrate heterogeneous tasks, and transfer knowledge across studies.

References

- [1] Guillaume Alain and Yoshua Bengio. Understanding intermediate layers using linear classifier probes. *arXiv preprint arXiv:1610.01644*, 2016. 6
- [2] Badr AlKhamissi, Greta Tuckute, Yingtian Tang, Taha Osama A Binhuraib, Antoine Bosselut, and Martin Schrimpf. From language to cognition: How llms outgrow the human language network. In *Proceedings of the 2025 Conference on Empirical Methods in Natural Language Processing*, pages 24332–24350, 2025. 2
- [3] Hasan A Bedel, Irmak Sivgin, Onat Dalmaz, Salman UH Dar, and Tolga Çukur. Bolt: Fused window transformers for fmri time series analysis. *Medical image analysis*, 88: 102841, 2023. 1
- [4] Tom Brown, Benjamin Mann, Nick Ryder, Melanie Subbiah, Jared D Kaplan, Prafulla Dhariwal, Arvind Neelakantan, Pranav Shyam, Girish Sastry, Amanda Askell, et al. Language models are few-shot learners. *Advances in neural information processing systems*, 33:1877–1901, 2020. 1
- [5] Josue Ortega Caro, Antonio Henrique de Oliveira Fonseca, Syed A Rizvi, Matteo Rosati, Christopher Averill, James L Cross, Prateek Mittal, Emanuele Zappala, Rahul Madhav Dhodapkar, Chadi Abdallah, et al. Brainlm: A foundation model for brain activity recordings. In *The Twelfth International Conference on Learning Representations*. 1, 2, 3, 7
- [6] ADHD-200 consortium. The adhd-200 consortium: a model to advance the translational potential of neuroimaging in clinical neuroscience. *Frontiers in systems neuroscience*, 6: 62, 2012. 6
- [7] Jacob Devlin, Ming-Wei Chang, Kenton Lee, and Kristina Toutanova. Bert: Pre-training of deep bidirectional transformers for language understanding. In *Proceedings of the 2019 conference of the North American chapter of the association for computational linguistics: human language technologies, volume 1 (long and short papers)*, pages 4171–4186, 2019. 3
- [8] Adriana Di Martino, David O’connor, Bosi Chen, Kaat Alaerts, Jeffrey S Anderson, Michal Assaf, Joshua H Balmers, Leslie Baxter, Anita Beggato, Sylvie Bernaerts, et al. Enhancing studies of the connectome in autism using the autism brain imaging data exchange ii. *Scientific data*, 4(1): 1–15, 2017. 6
- [9] Zijian Dong, Ruilin Li, Yilei Wu, Thuan Tinh Nguyen, Joanna Chong, Fang Ji, Nathanael Tong, Christopher Chen, and Juan Helen Zhou. Brain-jepa: Brain dynamics foundation model with gradient positioning and spatiotemporal masking. *Advances in Neural Information Processing Systems*, 37:86048–86073, 2024. 1, 2, 3, 7
- [10] Jennifer Stine Elam, Matthew F Glasser, Michael P Harms, Stamatiou N Sotiropoulos, Jesper LR Andersson, Gregory C Burgess, Sandra W Curtiss, Robert Oostenveld, Linda J Larson-Prior, Jan-Mathijs Schoffelen, et al. The human connectome project: a retrospective. *NeuroImage*, 244:118543, 2021. 6
- [11] Yaroslav Ganin, Evgeniya Ustinova, Hana Ajakan, Pascal Germain, Hugo Larochelle, François Laviolette, Mario March, and Victor Lempitsky. Domain-adversarial training of neural networks. *Journal of machine learning research*, 17(59):1–35, 2016. 4
- [12] Aaron Gokaslan, Vanya Cohen, Ellie Pavlick, and Stefanie Tellex. Openwebtext corpus. <http://SkyLion007.github.io/OpenWebTextCorpus>, 2019. 4
- [13] Edward J Hu, Yelong Shen, Phillip Wallis, Zeyuan Allen-Zhu, Yuanzhi Li, Shean Wang, Lu Wang, Weizhu Chen, et al. Lora: Low-rank adaptation of large language models. *ICLR*, 1(2):3, 2022. 4, 6, 8
- [14] Wei-Bang Jiang, Yansen Wang, Bao-Liang Lu, and Dongsheng Li. Neurolm: A universal multi-task foundation model for bridging the gap between language and eeg signals. *arXiv preprint arXiv:2409.00101*, 2024. 1, 4, 5
- [15] Wei-Bang Jiang, Li-Ming Zhao, and Bao-Liang Lu. Large brain model for learning generic representations with tremendous eeg data in bci. *arXiv preprint arXiv:2405.18765*, 2024. 1
- [16] Xuan Kan, Hejie Cui, Joshua Lukemire, Ying Guo, and Carl Yang. Fbnetgen: Task-aware gnn-based fmri analysis via functional brain network generation. In *International conference on medical imaging with deep learning*, pages 618–637. PMLR, 2022. 2, 7
- [17] Xuan Kan, Wei Dai, Hejie Cui, Zilong Zhang, Ying Guo, and Carl Yang. Brain network transformer. *Advances in Neural Information Processing Systems*, 35:25586–25599, 2022. 1, 2, 7
- [18] Nicole R Karcher and Deanna M Barch. The abcd study: understanding the development of risk for mental and physical health outcomes. *Neuropsychopharmacology*, 46(1):131–142, 2021. 5, 6
- [19] Jeremy Kawahara, Colin J Brown, Steven P Miller, Brian G Booth, Vann Chau, Ruth E Grunau, Jill G Zwicker, and Ghassan Hamarneh. Brainnetcnn: Convolutional neural networks for brain networks; towards predicting neurodevelopment. *NeuroImage*, 146:1038–1049, 2017. 1, 2, 3, 7
- [20] Peter Kim, Junbeom Kwon, Sunghwan Joo, Sangyoon Bae, Donggyu Lee, Yoonho Jung, Shinjae Yoo, Jiok Cha, and Taesup Moon. Swift: Swin 4d fmri transformer. *Advances in Neural Information Processing Systems*, 36:42015–42037, 2023. 1, 2, 7
- [21] Chunyuan Li, Cliff Wong, Sheng Zhang, Naoto Usuyama, Haotian Liu, Jianwei Yang, Tristan Naumann, Hoifung Poon, and Jianfeng Gao. Llava-med: Training a large language-and-vision assistant for biomedicine in one day. *Advances in Neural Information Processing Systems*, 36:28541–28564, 2023. 1
- [22] Junnan Li, Dongxu Li, Silvio Savarese, and Steven Hoi. Blip-2: Bootstrapping language-image pre-training with frozen image encoders and large language models. In *International conference on machine learning*, pages 19730–19742. PMLR, 2023. 1
- [23] Xiaoxiao Li, Yuan Zhou, Nicha Dvornek, Muhan Zhang, Siyuan Gao, Juntang Zhuang, Dustin Scheinost, Lawrence H

- Staib, Pamela Ventola, and James S Duncan. Braingnn: Interpretable brain graph neural network for fmri analysis. *Medical Image Analysis*, 74:102233, 2021. 1, 2, 7
- [24] Aixin Liu, Bei Feng, Bing Xue, Bingxuan Wang, Bochao Wu, Chengda Lu, Chenggang Zhao, Chengqi Deng, Chenyu Zhang, Chong Ruan, et al. Deepseek-v3 technical report. *arXiv preprint arXiv:2412.19437*, 2024. 5
- [25] Fabian Mentzer, David Minnen, Eirikur Agustsson, and Michael Tschannen. Finite scalar quantization: Vq-vae made simple. *arXiv preprint arXiv:2309.15505*, 2023. 2, 6
- [26] Karla L Miller, Fidel Alfaro-Almagro, Neal K Bangerter, David L Thomas, Essa Yacoub, Junqian Xu, Andreas J Bartsch, Saad Jbabdi, Stamatiou N Sotiropoulos, Jesper LR Andersson, et al. Multimodal population brain imaging in the uk biobank prospective epidemiological study. *Nature neuroscience*, 19(11):1523–1536, 2016. 5, 6
- [27] Ronald Carl Petersen, Paul S Aisen, Laurel A Beckett, Michael C Donohue, Anthony Collins Gamst, Danielle J Harvey, CR Jack Jr, William J Jagust, Leslie M Shaw, Arthur W Toga, et al. Alzheimer’s disease neuroimaging initiative (adni) clinical characterization. *Neurology*, 74(3): 201–209, 2010. 6
- [28] Weikang Qiu, Zheng Huang, Haoyu Hu, Aosong Feng, Yujun Yan, and Rex Ying. Mindllm: A subject-agnostic and versatile model for fmri-to-text decoding. *arXiv preprint arXiv:2502.15786*, 2025. 2
- [29] Alec Radford, Jeffrey Wu, Rewon Child, David Luan, Dario Amodei, Ilya Sutskever, et al. Language models are unsupervised multitask learners. *OpenAI blog*, 1(8):9, 2019. 6
- [30] Alexander Schaefer, Ru Kong, Evan M Gordon, Timothy O Laumann, Xi-Nian Zuo, Avram J Holmes, Simon B Eickhoff, and BT Thomas Yeo. Local-global parcellation of the human cerebral cortex from intrinsic functional connectivity mri. *Cerebral cortex*, 28(9):3095–3114, 2018. 3, 5
- [31] Guobin Shen, Dongcheng Zhao, Yiting Dong, Qian Zhang, and Yi Zeng. Alignment between brains and ai: Evidence for convergent evolution across modalities, scales and training trajectories. *arXiv preprint arXiv:2507.01966*, 2025. 2
- [32] Sheng Shen, Shijia Yang, Tianjun Zhang, Bohan Zhai, Joseph E Gonzalez, Kurt Keutzer, and Trevor Darrell. Multitask vision-language prompt tuning. In *Proceedings of the IEEE/CVF Winter Conference on Applications of Computer Vision*, pages 5656–5667, 2024. 5
- [33] Ye Tian, Daniel S Margulies, Michael Breakspear, and Andrew Zalesky. Topographic organization of the human sub-cortex unveiled with functional connectivity gradients. *Nature neuroscience*, 23(11):1421–1432, 2020. 3, 5
- [34] Aaron Van Den Oord, Oriol Vinyals, et al. Neural discrete representation learning. *Advances in neural information processing systems*, 30, 2017. 2, 4, 6
- [35] Yuxiang Wei, Yanteng Zhang, Xi Xiao, Tianyang Wang, Xiao Wang, and Vince D Calhoun. 4d multimodal co-attention fusion network with latent contrastive alignment for alzheimer’s diagnosis. *arXiv preprint arXiv:2504.16798*, 2025. 1, 3
- [36] Weihao Xia, Raoul de Charette, Cengiz Oztireli, and Jing-Hao Xue. Umbrae: Unified multimodal brain decoding. In *European Conference on Computer Vision*, pages 242–259. Springer, 2024. 2
- [37] Xi Xiao, Yunbei Zhang, Xingjian Li, Tianyang Wang, Xiao Wang, Yuxiang Wei, Jihun Hamm, and Min Xu. Visual instance-aware prompt tuning. *arXiv preprint arXiv:2507.07796*, 2025. 1
- [38] Jiaying Xu, Kai He, Yue Tang, Wei Li, Mengcheng Lan, Xia Dong, Yiping Ke, and Mengling Feng. Brainprompt: Multi-level brain prompt enhancement for neurological condition identification. In *International Conference on Medical Image Computing and Computer-Assisted Intervention*, pages 172–182. Springer, 2025. 3
- [39] Yanwu Yang, Chenfei Ye, Guinan Su, Ziyao Zhang, Zhikai Chang, Hairui Chen, Piu Chan, Yue Yu, and Ting Ma. Brainmass: Advancing brain network analysis for diagnosis with large-scale self-supervised learning. *IEEE transactions on medical imaging*, 43(11):4004–4016, 2024. 7
- [40] Xiaohua Zhai, Basil Mustafa, Alexander Kolesnikov, and Lucas Beyer. Sigmoid loss for language image pre-training. In *Proceedings of the IEEE/CVF international conference on computer vision*, pages 11975–11986, 2023. 4